Solar Phys (2008) 253: 133–141
DOI 10.1007/s11207-008-9278-5

Solar Radio Spikes in 2.6 – 3.8 GHz during the 13 December 2006 Event

S.J. Wang · Y.H. Yan · Y.Y. Liu · Q.J. Fu · B.L. Tan · Y. Zhang

Received: 30 November 2007 / Accepted: 13 October 2008 / Published online: 4 November 2008

Abstract On 13 December 2006, some unusual radio bursts in the range 2.6 – 3.8 GHz were observed during an X3.4 flare/CME event from 02:30 to 04:30 UT in active region NOAA 10930 (S06W27) with the digital spectrometers of the National Astronomical Observatories of China (NAOC). During this event many spikes were detected with the high temporal resolution of 8 ms and high frequency resolution of 10 MHz. Many of them were found to have complex structures associated with other radio burst types. The new observational features may reflect certain emission signatures of the electron acceleration site. In this paper, we present the results of the analysis of the new observational features of the complex spikes. According to the observed properties of the spikes, we identify five classes. Their observational parameters, such as duration, bandwidth, and relative bandwidth, were determined. Most spikes had negative polarization, but spikes with positive polarization were observed during a short time interval and were identified as a separate class. Based on the analysis of observations with *Hinode*/SOT (Solar Optical Telescope) we suggest that the sources of the spikes with opposite polarizations were different. Combined observations of spikes and fiber bursts are used to estimate the magnetic field strength in the source.

Keywords Sun · Flare · Radio emission · Spikes

1. Introduction

Solar radio spikes represent one type of fine temporal structures with extreme characteristics including very high brightness temperature (up to 10^{15} K), very short duration (less than 0.1 s), very narrow bandwidth (relative frequency bandwidth $\Delta f/f < 10\%$), and generally high polarization. They usually appear in clusters as impulsive radio emission and occupy

Radio Physics and the Flare-CME Relationship
Guest Editors: Karl-Ludwig Klein and Silja Pohjolainen

S.J. Wang (✉) · Y.H. Yan · Y.Y. Liu · Q.J. Fu · B.L. Tan · Y. Zhang
National Astronomical Observatories, Chinese Academy of Sciences, Beijing 100012, People's Republic of China
e-mail: wsj@bao.ac.cn

a given frequency range with a total duration that is generally shorter than several minutes. Some spikes develop in the earlier phase of flares, whereas some of them develop in the later phase probably when the events are intense. They can be present in a very large spectral range from 200 MHz up to 8 GHz (Bastian, Benz, and Gary, 1998; Wang and Xie, 1999; Wang, Yan, and Fu, 2001, 2002; Fleishman and Mel'nikov, 1998). Spikes are often associated in time with both type III bursts and hard X-ray bursts. All of them may give some information about energetic electrons in the solar corona (Benz and Kane, 1986).

Solar Broadband Radio Spectrometers (SBRS) in the microwave band began routine observations after June 2000 at Huairou Station of the National Astronomical Observatories (NAOC), Chinese Academy of Sciences (CAS) (Fu *et al.*, 2004). During the event on 13 December 2006, many radio spikes in the range 2.6 – 3.8 GHz were observed with high resolution (10 MHz and 8 ms) using these digital spectrometers. We classify these spikes in five classes, one of them because of its positive polarization and the other four classes based on their appearances in the dynamic spectrum. From the data we determined the observational parameters of the spikes. The third class of spikes appeared accompanied by radio fibers. We discuss this class of spikes in detail because of their magnetic field strength and the spatial scale of their sources.

2. Observations

On 13 December 2006, an X3.4 flare/CME was observed around 2:00 – 4:00 UT in active region (AR) NOAA 10930 at S06W27. During this time interval, many spikes were detected superposed on the radio continuum in the frequency range 2.6 – 3.8 GHz by the digital spectrometers of NAOC. We show the radio emission of the event in Figure 1. The spikes were found to have complex structures associated with other radio burst signatures. Different types of radio bursts are generally believed to result from different emission mechanisms. Therefore, we classify these microwave spikes into five classes, one of them because of its positive polarization, and the other four classes based on their association with different types of radio bursts. Almost all spike clusters during this event had negative polarization except class (1); this particular class will be discussed in Section 4.1 in detail.

Figure 1(a) shows the time profile at 2.84 GHz during the entire event. Each number (1, 2, 3, 4, and 5) inside a circle corresponds to each of the five classes of spikes. The 12 numbers (1 – 12) indicate the peaks of the radio emission. Figure 1(b) shows the relevant radio spectrum in the frequency range 2.6 – 3.8 GHz. In class (1), the spikes with positive polarization occurred in the time interval 2:31:45 – 2:32:01 UT. Class (2) and (3) spikes were detected during three time intervals. The last two classes of spikes, (4) and (5), were observed during six time intervals (see Table 1).

We select one segment lasting 5 seconds for each class of spikes; then, we arrange the five selected segments in Figure 2. Their characteristics are as follows:

1. Spikes with positive polarization, which are obviously different from others with negative polarization that were observed before and after them [see Figure 2(a)];
2. Spikes accompanied with a bright patch of emission (duration $\Delta t \sim 1.5$ s, bandwidth $\Delta f \sim 650$ MHz) that had a well-defined boundary in the dynamic spectrum [see Figure 2(b)];
3. Spikes accompanied with fibers (intermediate drift bursts; see Young *et al.*, 1961) that are superposed on solar type IV continua [see Figure 2(c)];
4. Spikes arranged as zebra patterns, emission strips or fibers [see Figure 2(d)]; and
5. Irregular spikes that appear superposed on the background emissions [see Figure 2(e)].

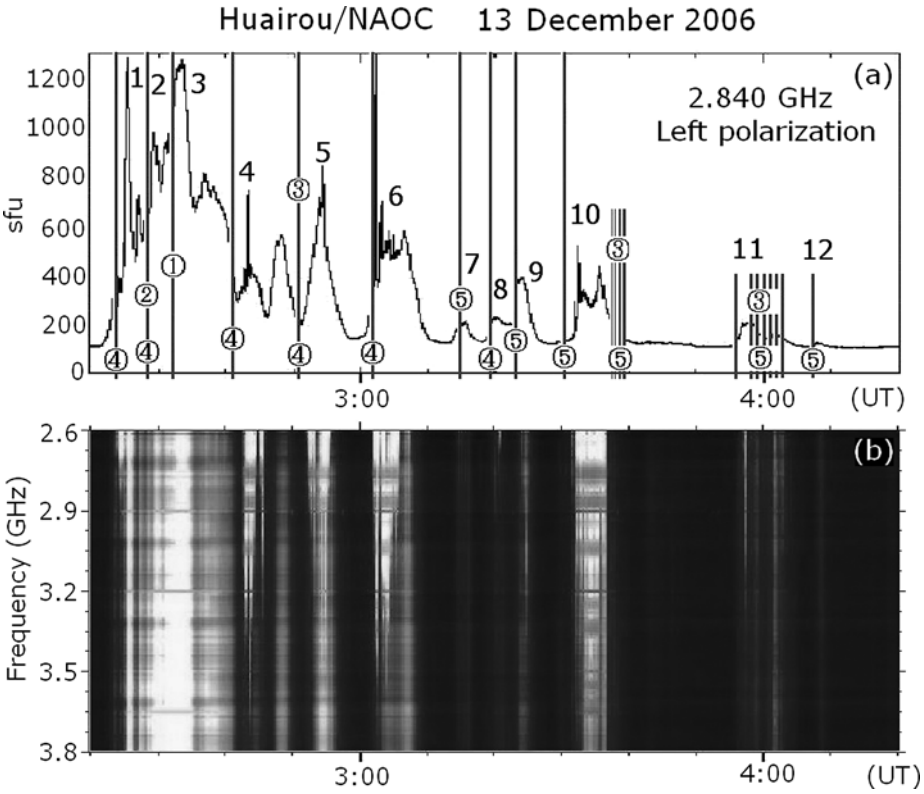

Figure 1 Radio emission of the event on 13 December 2006. (a) Time profile of the radio emission at 2.84 GHz during the entire event. Each number (1 – 5) inside a circle corresponds to each of the five classes of spikes. The numbers (1 – 12) indicate the 12 peaks of the radio emission. (b) Relevant radio spectrum in the range 2.6 – 3.8 GHz.

3. Observational Parameters

All the spikes in this event were grouped in clusters. We used the method reported in our former work (Wang, Yan, and Fu, 2002) to analyze these spikes. Some observational parameters, such as frequency drift rate, duration, bandwidth, and relative bandwidth, were determined. We summarize the ranges of the parameters, which are the measured lower and upper limits, in Table 1.

The absolute errors of measured duration and bandwidth are identical to the temporal and frequency resolutions of the spectrometer: 8 ms and 10 MHz. The absolute errors of the relative bandwidth and the frequency drift rate ($E_{\rm rb}$ and $E_{\rm fd}$) that are caused by the uncertainties of the measured frequency (f), bandwidth (Δf), and duration (Δt) are estimated and averaged. Then the mean absolute error divided by the average value gives the average relative error. The average absolute errors and average relative errors are shown in the last two lines of Table 1.

We find that the lower limit of spike duration is identical to the temporal resolution of the spectrometer (8 ms) and the lower limit of spike bandwidth is close to the frequency

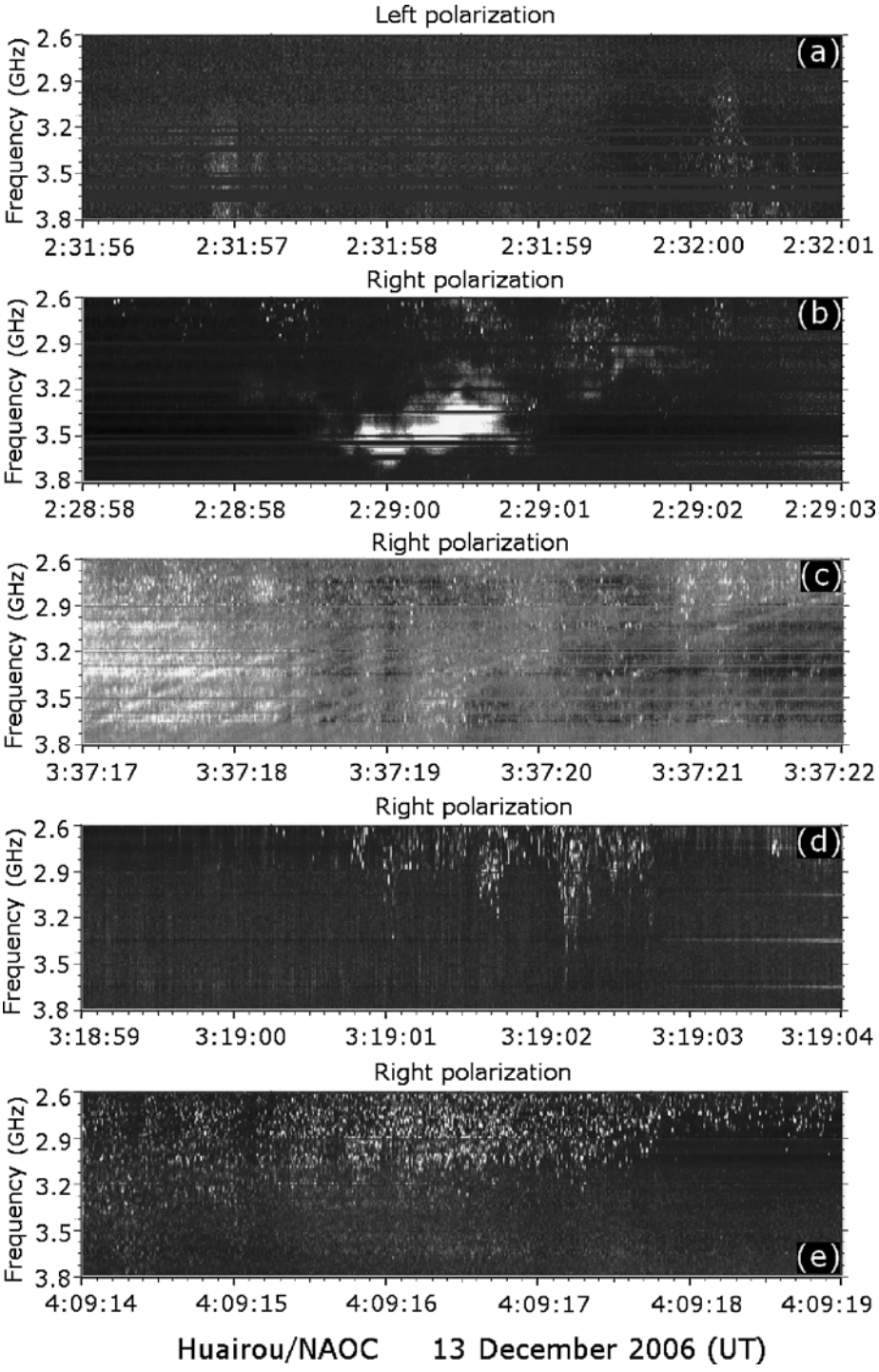

Figure 2 Examples of the five classes of solar radio spikes on 13 December 2006. Each segment lasts 5 seconds.

Table 1 Parameters of the five kinds of radio spikes.

Class	Range (GHz)	Time (UT)	Duration (ms)	Bandwidth (BW) (MHz)	Relative (%)	|Drift| (GHz s^{-1})
(1)	2.71 – 3.80	2:31:45 – 2:32:01	8–32	20–90	0.53 – 2.40	2.81 – 3.75
(2)-a[a]	2.60 – 3.80	2:28:53 – 2:28:56	8–40	30–130	0.86 – 4.91	3.25 – 5.00
(2)-b	2.60 – 3.80	2:28:58 – 2:29:03	8–40	10–110	0.31 – 4.14	2.75 – 5.00
(2)-c	2.60 – 3.30	2:29:08 – 2:29:10	8–48	20–220	0.68 – 7.17	4.58 – 6.25
(3)-a[b]	2.60 – 3.05	2:50:25 – 2:50:28	8–32	20–190	0.74 – 6.95	5.94 – 8.75
(3)-b	2.60 – 3.80	3:36:59 – 3:37:26	8–48	30–80	0.80 – 2.19	1.67 – 3.75
(3)-c	2.60 – 3.51	3:58:47 – 3:58:55	8–32	30–110	0.83 – 3.88	3.44 – 5.00
(4)-a	2.60 – 3.41	2:23:35 – 2:23:37	8–48	10–130	0.36 – 4.12	2.71 – 3.75
(4)-b	2.60 – 3.34	2:28:00 – 2:28:31	8–40	20–120	0.60 – 3.99	3.00 – 6.25
(4)-c	3.03 – 3.80	2:41:53 – 2:41:55	8–24	10–70	0.29 – 1.97	2.92 – 5.00
(4)-d	2.91 – 3.80	2:52:18 – 2:52:24	8–48	20–190	0.59 – 5.63	3.96 – 7.50
(4)-e	3.22 – 3.80	3:02:44 – 3:02:58	8–32	30–100	0.81 – 2.80	3.13 – 6.25
(4)-f	2.60 – 3.70	3:18:53 – 3:19:02	8–32	20–70	0.59 – 2.30	2.19 – 5.00
(5)-a	2.60 – 3.67	3:13:02 – 3:13:11	8–24	10–40	0.29 – 1.40	1.67 – 3.75
(5)-b	2.79 – 3.80	3:23:13 – 3:23:27	8–24	10–30	0.29 – 0.90	1.25 – 5.00
(5)-c	2.60 – 3.37	3:30:20 – 3:30:27	8–24	10–40	0.30 – 1.27	1.67 – 5.00
(5)-d	2.60 – 3.66	3:39:00 – 3:39:12	8–48	20–70	0.60 – 2.30	1.46 – 3.75
(5)-e	2.60 – 3.80	3:59:57 – 4:00:07	8–32	30–130	0.81 – 4.79	4.06 – 6.25
(5)-f	2.60 – 3.80	4:09:09 – 4:09:24	8–48	30–170	0.83 – 7.54	3.54 – 7.50
Average value			8–36	20–110	0.60 – 3.66	2.95 – 5.40
Average absolute error			8–8	10–10	0.30 – 0.34	0.99 – 6.65
Average relative error			100.0–22.2(%)	50.0–9.1(%)	50.0 – 9.3(%)	33.6 – 123.1(%)

[a]For class (2), in a very narrow time interval, there were three clusters of spikes [only one time position in Figure 1(a)]. We label them as (2)-a, (2)-b, and (2)-c.

[b]For classes (3) – (5), Figure 1(a) shows all clusters of spikes in time sequence. Accordingly, we label them as (a – f).

resolution of the spectrometer (10 MHz). Therefore the errors of lower limits including the duration, bandwidth, and relative bandwidth and the error of upper limits of frequency drift rate are very high and depend strongly on the resolutions of the spectrometer. The average upper limits of lifetime, bandwidth, and relative bandwidth of the spikes were 36 ms, 110 MHz, and 3.66%, respectively, and the average lower limit of frequency drift rate was 2.95 GHz s^{-1}. The polarization degrees of the spikes in this event were very high, near 100%.

In Figure 1, we mark the clusters of spikes within each class using vertical lines and we show their characteristics in Table 1. There were 12 radio peaks marked from 1 to 12 in Figure 1. All the spike clusters occurred before those radio peaks. The time differences between them are shown in Table 2. The average value of the delay time is about 1.53 minutes.

Spikes in the third class appear accompanied by radio fibers. The observational parameters, their statistical averages, and errors of the fiber bursts are summarized in Table 3.

Table 2 Time difference Δt_{sr} of the spikes before the relevant radio peaks.

Number	Δt_{sr} (min)	Number	Δt_{sr} (min)	Number	Δt_{sr} (min)
1	1.9	5	4.0	9	1.2
2	0.9	6	0.3	10	2.2
3	1.8	7	0.6	11	1.1
4	2.7	8	0.8	12	0.9
Average of Δt_{sr}:		1.53 min			

Table 3 Parameters of the fiber structures that accompanied the spikes in class (3).

Group	Duration (ms)	Bandwidth (BW) (MHz)	Relative BW (%)	Drift (MHz s^{-1})
(a)	248−600	160−340	5.71−12.06	(+) 473 − 690
(b)	408−1536	130−480	3.68−13.99	(−) 259 − 345
(c)	264−1160	250−850	7.97−25.41	(+) 625 − 947
Average	307−1099	180−557	5.79−17.15	452 − 661
Average absolute error	8−8	10−10	0.34−0.37	26 − 43
Average relative error	2.6−0.7(%)	5.6−1.8(%)	5.9−2.2(%)	5.8 − 6.5(%)

4. Discussion and Conclusions

4.1. Spikes with Positive Polarization

In this event, almost all the radio bursts and fine structures had a negative polarization. There were only two time intervals when the radio bursts had a positive polarization: 2:31:45 – 2:32:01 UT and 3:04:07 – 3:04:08 UT. In the first time interval, 2:31:45 – 2:32:01 UT, there were three groups of spikes with positive polarization [with two groups of spikes being shown in Figure 2(a)]. Although the positive or negative polarizations themselves do not determine the physical nature of the spike sources, the spikes with positive polarization indicated obviously a source region or radiation mechanism that was different from the other radio bursts (including the other spikes) and was active for less than 1 minute. Therefore, we classified them as class (1).

As is well known, the change of radio polarization could be interpreted as the effect of the change of angle between the line of sight and the magnetic field direction (Kruger, 1979). This change comes from a change of source or a change in the magnetic field. Then, we analyzed observations by *Hinode*/SOT (Solar Optical Telescope) (Kosugi *et al.*, 2007; Tsuneta *et al.*, 2008). (There are no other high-cadence data available in this time interval.) As indicated by the black rectangle in Figure 3, we find that a SOT brightening suddenly occurred at 2:30:39 UT. This was a short-lived feature. The time at which the brightening appeared agreed with the time of the spikes with positive polarization. The SOT brightening could correspond to the region where the sources of the spikes with positive polarization were located. Therefore, the sources of the spikes with positive polarization were probably different from those with negative polarization.

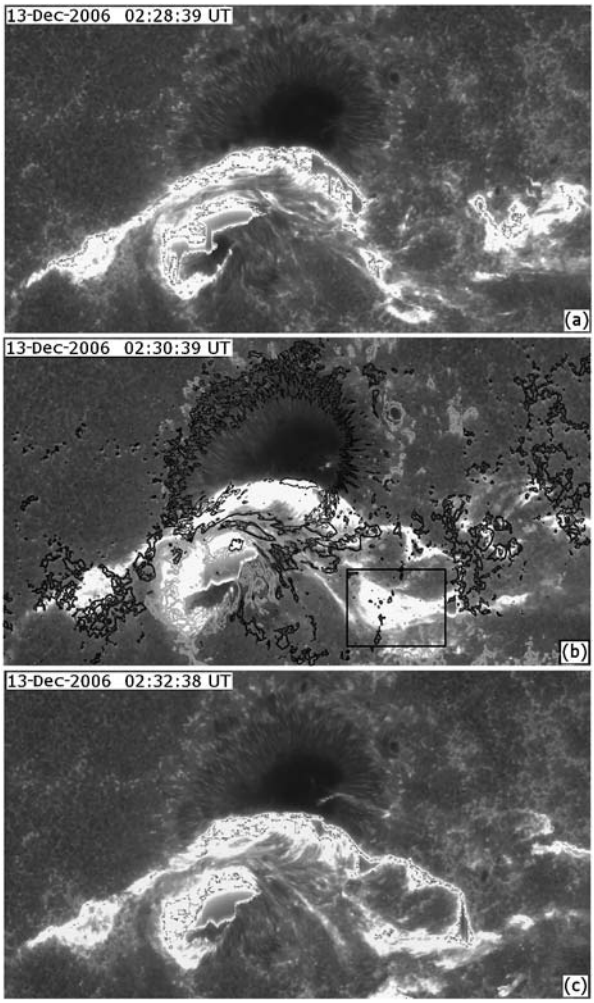

Figure 3 *Hinode*/SOT images (Ca II H) for active region NOAA 10930 from 02:28:39 UT to 02:32:38 UT showing a sudden brightening at 2:30:39 UT indicated by the black rectangle. In (b) contours of the SOT/NFI magnetogram (Fe I 6302.5 Å) are overlaid on the SOT image at 2:30:39 UT, the contour lines are drawn at ±300, 500, and 800 Gauss, and the bright and dark contours represent the positive and negative polarities, respectively.

4.2. Magnetic Field

The polarization degree of the spikes was very high, close to 100%. Electron cyclotron maser emission at any harmonic, as well as fundamental plasma emission, produces strongly (100%) polarized radio emission, whereas plasma emission at the second harmonic is moderately or weakly polarized. Furthermore, when we overlaid the contours of the SOT/NFI (Narrowband Filter Imager) magnetogram (Fe I 6302.5 Å) on the SOT Ca II H image at 2:30:39 UT in Figure 3(b), we found that the magnetic field in the black rectangle was weaker. It was difficult to determine the magnetic field orientation at the place of the new SOT source. Thus, we consider that the spikes are generated by electron cyclotron maser (ECM) microwave emission. Such emission occurs at discrete harmonics of the gyrofrequency, $f_b = 2.8B$ (MHz) (White *et al.*, 1995). We, thus, have

$$f = sf_b = 2.8sB \quad \text{(MHz)}, \tag{1}$$

where f is the frequency of the ECM emission, f_b is the electron gyrofrequency, s is the harmonic number (1, 2, 3, ...), and B is the magnetic field strength in Gauss. For the ECM instability, the x-mode at the second harmonic would be predominant in its growth rate (Winglee and Dulk, 1986). When the frequency of the ECM emission f equals the observing frequency (central frequency around 3.2 GHz for the groups of radio spikes), we obtain an approximate magnetic field strength of 570 Gauss.

For the fiber structures, there are mainly two models that interpret the drift rate of the fiber bursts as corresponding to the Alfvén velocity or to the whistler group velocity (Aurass *et al.*, 2005). Here, we choose to estimate the magnetic field using the model of Alfvén solitons (Bernold and Treumann, 1983). From the Alfvén soliton model,

$$B = \frac{4\pi H \sqrt{m_e m_i}}{e} \frac{\mathrm{d}f}{\mathrm{d}t}, \tag{2}$$

where H is the barometric scale height, which we take as $H = 1 \times 10^4$ km, and $\mathrm{d}f/\mathrm{d}t$ is the average frequency drift rate, which was measured to be in the range of 452 – 661 MHz s^{-1} (Table 3), B was estimated to be about 460 – 680 Gauss for the source of the radio fibers.

4.3. Spatial Scale

In this section, we estimate the spatial scales of the spike source and the fiber source for class (3) and we compare them to find the relation between the spikes and fibers.

First, for the spikes, by assuming an emission frequency depending on a characteristic frequency, the upper limit (l) of the spike source size could be estimated by the following relation (Benz, 1986):

$$l = \lambda \frac{\Delta f}{f}, \tag{3}$$

where λ is the length corresponding to the characteristic magnetic scale. By taking $\lambda =$ 6000 km (Benz, 1985) and $\Delta f/f = 3.66\%$ (the average upper limit) for this event, the spatial scale of the spike sources could be estimated to be less than 220 km.

Then, for the fibers, following the work of Bernold and Treumann (1983), the radio flux emitted by one soliton and the volume (V_s) of a single soliton are

$$F(n_e, B) = \frac{3.2 \times 10^{-3} {B_0}^2}{\sqrt{n_e}} \quad \text{(sfu)} \tag{4}$$

and

$$V_s = \frac{3 \times 10^{12}}{\sqrt{n_e}} \quad (\text{cm}^3). \tag{5}$$

Taking $B_0 = 600$ G, $n_e = 3.2 \times 10^{10}$ cm^{-3} for $f = 3.2$ GHz, and the measured radio flux of about 400 sfu, we obtain the number of solitons contained in a single fiber source, $N =$ 4.12×10^{13}. Here $N = (F_0/F)\tau\Delta f$, where F_0 is the measured radio flux for the fibers, $\tau \sim 703$ ms is taken as the median of the average value of the duration of the fibers, and $\Delta f \sim 369$ MHz is taken as the median of the average value of the frequency bandwidth of the fibers (see Table 3). The volume of a single soliton is estimated to be about 5 m^3. The volume of the fiber source is $V = V_s N = 2.2 \times 10^5$ km^3. Taking a diameter of about 30 km for a single cylindrical fiber source (Wang and Zhong, 2006) gives its estimated length to be ~310 km.

Therefore, we have found that the estimated values for the spatial scale of the spike and fiber sources agree in order of magnitude.

4.4. Conclusions

In this event, almost all the radio bursts and fine structures had negative polarization. However, for less than 1 minute from 2:31:45 to 2:32:01 UT, three groups of spikes with positive polarization were present. We classify those spikes as class (1). After analyzing *Hinode*/SOT images, we suggest that the spikes with different polarization probably came from different source regions.

For class (3), the detected spikes were accompanied by fibers [Figure 2(c)]. We cannot say whether the spikes and the fibers came from the same region or not. Detection of the associated radio sources requires imaging observations, for example, radioheliographs working in the microwave band, which we will develop. However, the estimated values of the field strength for the spike and fiber sources are in agreement in order of magnitude. Their estimated spatial scales are also in agreement. This suggests that the two kinds of fine structures probably came from sources with similar physical conditions.

From Figure 1 and Table 2, it can be seen that all the spike clusters occurred before the radio peaks. This is in agreement with previous observational claims that spikes occur in the rise phase of centimeter radio bursts and, thus, are associated with major flares (Slottje, 1978), although Benz (2004) recently reported that clusters of narrowband decimetric radio spikes occurred in the decay phase of solar flares at low decimeter frequencies (327 – 430 MHz).

Acknowledgements This work was supported by the Ministry of Science and Technology of China (G2006CB806301), the National Nature Science Foundation of China (10333030), the Foundation of Chinese Academy of Sciences (KJCX2-YW-T-04), a cooperation project of NSFC-RFBR between China and Russia (10711120371). We are also grateful for the availability of *Hinode* online data. We wish to thank the anonymous referee for helpful advice on improving this paper.

References

Aurass, H., Rausche, G., Mann, G., Hofmann, A.: 2005, *Astron. Astrophys.* **435**, 1137.
Bastian, T.S., Benz, A.O., Gary, D.E.: 1998, *Annu. Rev. Astron. Astrophys.* **36**, 131.
Benz, A.O.: 1985, *Solar Phys.* **96**, 357.
Benz, A.O.: 1986, *Solar Phys.* **104**, 99.
Benz, A.O.: 2004. In: Gary, D.E., Keller, C.U. (eds.) *Solar and Space Weather Radiophysics: Current Status and Future Developments*, Kluwer, Dordrecht, 203.
Benz, A.O., Kane, S.R.: 1986, *Solar Phys.* **104**, 179.
Bernold, T.E.X., Treumann, R.A.: 1983, *Astrophys. J.* **264**, 677.
Fleishman, G.D., Mel'nikov, V.F.: 1998, *Phys.-Usp.* **41**, 1157.
Fu, Q.J., Ji, H.R., Qin, Z.H., Xu, Z.C., Xia, Z.G., Wu, H.A., Liu, Y.Y., Yan, Y.H., Huang, G.L., Chen, Z.J., *et al.*: 2004, *Solar Phys.* **222**, 167.
Kosugi, T., Matsuzaki, K., Sakao, T., Shimizu, T., Sone, Y., Tachikawa, S., Hashimoto, T., Minesugi, K., Ohnishi, A., Yamada, T., *et al.*: 2007, *Solar Phys.* **243**, 3.
Kruger, A.: 1979, *Introduction to Solar Radio Astronomy and Radio Physics*, Reidel, Dordrecht.
Slottje, C.: 1978, *Nature* **275**, 520.
Tsuneta, S., Ichimoto, K., Katsukawa, Y., Nagata, S., Otsubo, M., Shimizu, T., Suematsu, Y., Nakagiri, M., Noguchi, M., Tarbell, T., *et al.*: 2008, *Solar Phys.* **249**, 167.
Wang, M., Xie, R.X.: 1999, *Solar Phys.* **185**, 351.
Wang, S.J., Zhong, X.C.: 2006, *Solar Phys.* **236**, 155.
Wang, S.J., Yan, Y.H., Fu, Q.J.: 2001, *Astron. Astrophys.* **373**, 1083.
Wang, S.J., Yan, Y.H., Fu, Q.J.: 2002, *Solar Phys.* **209**, 185.
White, S.M., Kundu, M.R., Shimizu, T., Shibasaki, K., Enome, S.: 1995, *Astrophys. J.* **450**, 435.
Winglee, R.M., Dulk, G.A.: 1986, *Solar Phys.* **104**, 93.
Young, C.W., Spencer, C.L., Moreton, G.E., Roberts, J.A.: 1961, *Astrophys. J.* **133**, 243.